Materials & Design 207 (2021) 109850

Contents lists available at ScienceDirect

Materials & Design

journal homepage: www.elsevier.com/locate/matdes

High performance broadband self-driven photodetector based on MXene ($Ti_3C_2T_x$)/GaAs Schottky junction

Xiwei Zhang [a,*], Jiahua Shao [a,b], Chenxi Yan [a], Xinmiao Wang [a], Yufei Wang [a], Zhihui Lu [a], Ruijie Qin [a], Xiaowen Huang [c,*], Junlong Tian [a], Longhui Zeng [d]

[a] College of Physics and Electrical Engineering, Anyang Normal University, Anyang, Henan 455000, PR China
[b] School of Sciences, Henan University of Technology, Zhengzhou, Henan 450001, PR China
[c] State Key Laboratory of Biobased Material and Green Papermaking, Department of Bioengineering, Qilu University of Technology (Shandong Academy of Sciences), Jinan 250353, PR China
[d] Department of Applied Physics and Materials Research Center, The Hong Kong Polytechnic University, Hung Hom, Kowloon, Hong Kong, China

HIGHLIGHTS

- $Ti_3C_2T_x$/GaAs Schottky junction photodetector is prepared by simply dripping $Ti_3C_2T_x$ MXene solution on GaAs substrate.
- High responsivity of ~1.46 A/W, specific detectivity of ~1.23×10^{13} Jones are obtained when the device is operated in self-driven mode.
- The photodetector exhibits a broadband response spectrum up to 980 nm due to plasmon-induced hot electrons in $Ti_3C_2T_x$ MXene film.

GRAPHICAL ABSTRACT

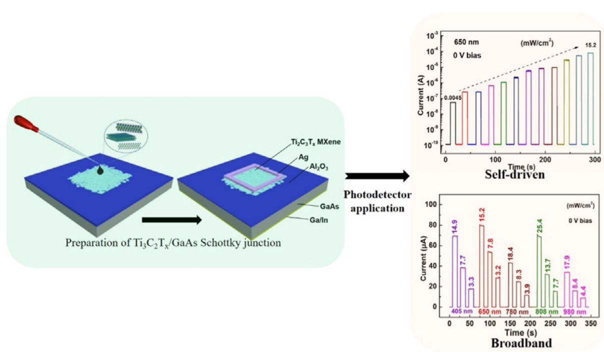

ARTICLE INFO

Article history:
Received 9 March 2021
Revised 18 May 2021
Accepted 23 May 2021
Available online 25 May 2021

Keywords:
$Ti_3C_2T_x$ MXene
GaAs
Schottky junction
Photodetector

ABSTRACT

As a novel family of 2D materials, MXenes are supposed to play a vital role in optoelectronic devices and systems due to their high conductivity, good optical properties, and favorable compatibility with water and organic solvents. However, the application of MXenes in highly sensitive photodetection is far scarcely investigated. Here, we demonstrate high-quality $Ti_3C_2T_x$/GaAs Schottky junction by simply dripping $Ti_3C_2T_x$ MXene solution on a pre-patterned GaAs substrate. Owing to the wide absorption of MXene and the good quality junction, the self-driven $Ti_3C_2T_x$/GaAs Schottky junction photodetector with an impressive performance is realized. The assembled photodetector exhibits a high sensitivity over a wide waveband with a good responsivity of ~1.46 A/W, a large specific detectivity of ~1.23×10^{13} Jones, and a high I_{light}/I_{dark} ratio of 5.6×10^5. Significantly, the photodetector is capable of sensing infrared light signal up to 980 nm which exceeds the absorption edge of GaAs (874 nm) due to the generation of hot electrons in $Ti_3C_2T_x$ MXene film. Given the superior device performance along with a simple and facile fabrication method, the $Ti_3C_2T_x$/GaAs Schottky junction photodetector may find the great potential in high performance broadband, self-driven photodetection applications.

* Corresponding authors.
E-mail addresses: xwezhang@outlook.com (X. Zhang), huangxiaowen2013@gmail.com (X. Huang).

https://doi.org/10.1016/j.matdes.2021.109850
0264-1275/

1. Introduction

Recently, a new class of two-dimensional (2D) materials, such as transition metal carbides, nitrides and carbon nitrides (MXenes), have attracted worldwide attention due to their rich chemical and physical properties [1–3]. The chemical formula of MXenes is $M_{n+1}X_nT_x$ (n = 1, 2, or 3), where M represents transition metal (e.g., Sc, Ti, Zr, Hf, Nb, Ta, Cr, Mo, Mn), X denotes C and/or N, T_x is surface functional group (e.g., hydroxyl, oxygen or fluorine) [4–7]. So far, over 30 different kinds of MXenes have been experimentally obtained and many more MXenes are theoretically predicted to exist [8–11]. MXenes have been found to demonstrate tailorable and excellent properties due to their abundant surface functional groups and stoichiometry. Especially, MXenes have been proved to have high optical transmittance in visible light region. $Ti_3C_2T_x$, in particular, has shown a transmittance of ~93% with a conductivity of ~5736 S cm^{-1} when its thickness is down to ~4 nm [12,13]. Also, the large tunability of work functions from ~2.14 eV to ~5.65 eV could be readily to achieve, covering a wide range of metals [14]. Benefiting from these appealing properties, outstanding photodetection performance has been demonstrated based on MXenes in previous studies [14,15]. Meanwhile, optical and electronic properties of MXenes are considered to be tailored by the surface terminations, transition metals, electrochemical intercalation, thickness and so on [16]. Consequently, these excellent optoelectronic properties, combined with hydrophilia, high transmittance, and high electrical conductivity make MXenes attractive and promising candidates for the important applications in optoelectronic devices and systems, such as energy storage and conversion devices [17], electromagnetic interference (EMI) shielding layer [18], transparent conductors [12,19], photovoltaic devices [9], light emitting diodes (LEDs) [20], photodetectors [14], etc.

Photodetector, as one of the most essential and important optoelectronic devices, can convert incident light into electrical signal, having wide-ranging applications including image sensing, night vision, communication and so on [21,22]. Thanks to their high conductivities, transparence, and hydrophily, the wide usage of MXenes in photodetectors has been demonstrated. For instance, Nabet et al. fabricated MXene-GaAs-MXene photodetectors by simply spin-coating transparent Ti_3C_2-based MXene electrodes on a purpose-designed GaAs in order to replace high-cost Au electrodes, which exhibited better photodetection performance than the counterpart device with Au electrode [23]. In addition, an all-sprayed-processable and large-area flexible photodetector by spraying both 2D $CsPbBr_3$ nanosheets and $Ti_3C_2T_x$ MXene on the paper substrate was assembled, and a high on/off ratio of ~2.3×10^3 as well as a fast response time of ~18 ms were obtained. Importantly, the flexible photodetector could still maintain an excellent stability after 1500 cycles bending operation [24]. Very recently, it has been reported that Mo_2CT_x, $Ti_3C_2T_x$, Nb_2CT_x, T_2CT_x, and V_2CT_x showed superior photodetection characteristics because of light-matter interaction in MXenes materials and dephasing of surface plasmon with a short lifetime in several studies [15]. Specially, all kinds of MXenes including Mo_2C, TiC, Ti_2CT_x combined with different semiconductors (e.g. MoS_2, TiO_2, ZnO, CdS, and Zn_2GeO_4) have been widely applied in high performance photodetectors, demonstrating the great potential in next-generation optoelectronic system applications [25–30].

Enlightened by these research works, we have developed a high-quality $Ti_3C_2T_x$/GaAs Schottky junction by simply dripping $Ti_3C_2T_x$ MXene solution on a pre-patterned GaAs substrate for a highly sensitive detection in multiband wavelength region. The assembled self-driven $Ti_3C_2T_x$/GaAs Schottky junction photodetector displays an excellent photodetection performance in term of a good responsivity of ~1.46 A/W, an impressive specific detectivity of ~1.23×10^{13} Jones, a high I_{light}/I_{dark} ratio of 5.6×10^5. Significantly, the photodetector exhibits a broadband response spectrum up to 980 nm which exceeds the absorption edge of GaAs due to the generated hot electrons in $Ti_3C_2T_x$ MXene film. These impressive findings together with a simple and facile preparation method make the present $Ti_3C_2T_x$/GaAs Schottky junction photodetector a building block for the further optoelectronic devices and systems applications.

2. Experimental section

Material Synthesis and Characterization: The $Ti_3C_2T_x$ MXene was synthesized from Ti_3AlC_2 MAX phase by etching the Al layers from the MAX phase (XFK01, XFK02, XFNANO). The morphologies of the obtained $Ti_3C_2T_x$ MXene was characterized by scanning electron microscope (SEM), and transmission electron microscopy (TEM). X-ray diffraction (XRD) and X-ray photoelectron spectroscopy (XPS) were used to study their structure and composition.

Device Fabrication and Characterization: To assemble $Ti_3C_2T_x$/GaAs Schottky junction, a ~80 nm Al_2O_3 insulating layer was firstly deposited on a rinsed n-type GaAs substrate (0.5×10^{-3}–10^{-3} Ω cm, ⟨100⟩) using photolithography and atomic layer deposition techniques to form a window (0.5 cm × 0.5 cm). Then the prepared $Ti_3C_2T_x$ MXene solution (XFK02, few layer nanoflakes) was dropped on the well-defined GaAs substrate. After naturally drying at room temperature in the air, Ag paste was painted at the edge of $Ti_3C_2T_x$ MXene film while In/Ga alloy as paste was painted on the back side of *n*-type GaAs as the electrode for measurement. Furthermore, the electrical and photoresponse measurements of the device were conducted at room temperature by a semiconductor characterization system (Keithley 4200) attached with different laser diodes (405, 650, 780, 808, 980 nm). The temperature-dependent electrical measurement was carried out by a Keithley 2636B source meter (Tektronix, USA) attached with a physical property measurement system (VersaLab, Quantum Design).

3. Results and discussion

Fig. 1a shows the typical SEM image of $Ti_3C_2T_x$ MXene (multilayer nanoflakes, XFK01), which reveals an accordion-like multilayered nanostructure with abundant open edges, indicating the successful synthesis of $Ti_3C_2T_x$ MXene. According to TEM image of $Ti_3C_2T_x$ MXene in Fig. 1b, the few layer $Ti_3C_2T_x$ nanoflakes have a lateral size of several hundreds of nanometers with clean and flat surface. In Fig. 1c, the XRD studies reveal that the five diffraction peaks located 6.77°, 21.48°, 34.30°, 41.85°, 61.00° can be indexed to the (002), (006), (101), (105) and (110) crystal planes of $Ti_3C_2T_x$ MXene, while the peak of (104) was not observed, indicating the successful preparation of few layer $Ti_3C_2T_x$ MXene and the existence of surface functional groups [3,31]. In addition, Fig. 1d-e shows XPS spectra of Ti 2p and C 1s core levels. For Ti 2p spectra, it consists of two peaks located at 454.8 eV ($Ti2p_{3/2}$) and 460.7 eV ($Ti2p_{1/2}$), indicating the bonding energy between Ti and C in $Ti_3C_2T_x$ MXene, respectively [9,32]. Besides, two peaks at 280.7 eV and 285.1 eV in the C1s core levels are considered to be related to Ti—C bond and C—C bond, respectively (Fig. 1e) [33]. All these basic characterizations collectively confirm that the few-layer $Ti_3C_2T_x$ nanoflakes with high quality were successfully obtained from a simple and general etching approach.

Fig. 2a schematically presents the crystal structure of $Ti_3C_2T_x$ MXene and the step-wising fabrication process of $Ti_3C_2T_x$/GaAs Schottky junction device are shown in Fig. 2b–d. Next, we studied the electrical characteristics of the $Ti_3C_2T_x$/GaAs Schottky junction. Fig. 3a shows the typical current–voltage (*I-V*) characteristic curve

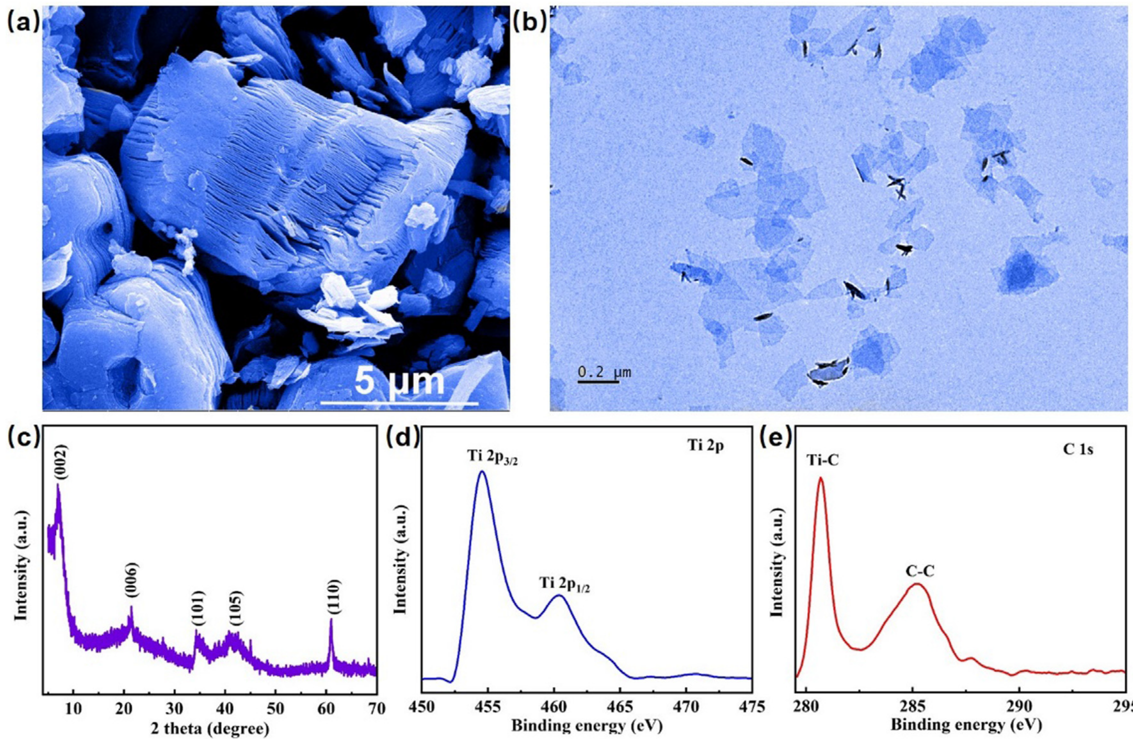

Fig. 1. (a) Typical SEM image of $Ti_3C_2T_x$ multilayer nanoflakes. (b) The representative TEM image of $Ti_3C_2T_x$ few layer nanoflakes. (c) XRD pattern of $Ti_3C_2T_x$ MXene. (d-e) Ti2p and C1s XPS spectra of $Ti_3C_2T_x$ MXene, respectively.

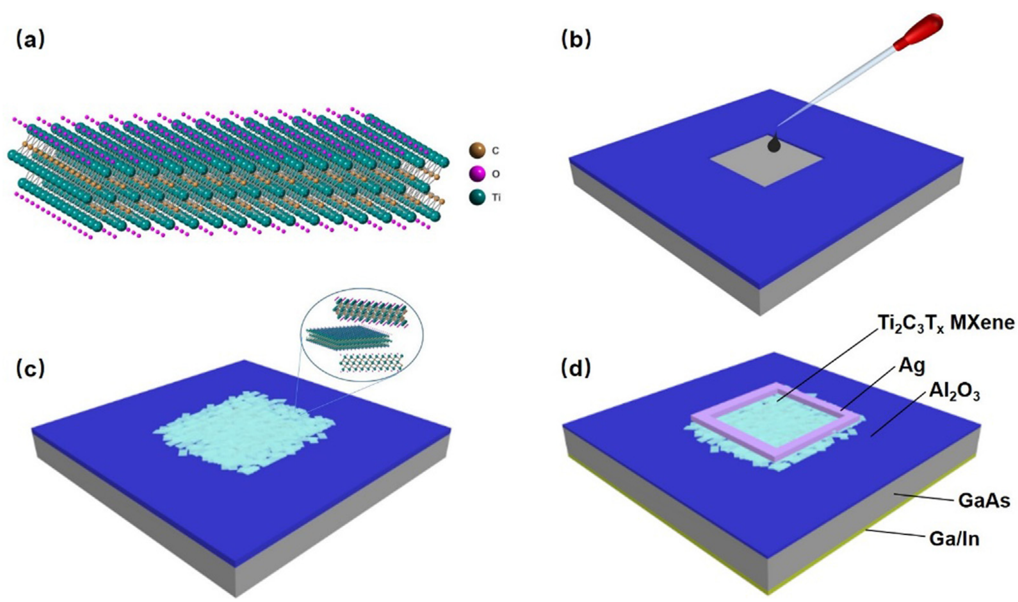

Fig. 2. (a) The schematic of the $Ti_3C_2T_x$ MXene. (b) - (d) The step-wising fabrication process of $Ti_3C_2T_x$/GaAs Schottky junction device.

of $Ti_3C_2T_x$/GaAs Schottky junction in the dark at room temperature. In addition, the inset of Fig. 3a depicts the cross-sectional schematic of the device and the semi-logarithmic *I-V* curve. One can easily find that the device exhibits a pronounced rectifying behavior with a high rectification ratio of ~55 at ± 1 V due to the formation of Schottky junction at $Ti_3C_2T_x$/GaAs interface. The *I-V* characteristic of the $Ti_3C_2T_x$/GaAs Schottky junction is studied by using the following equation:

$$I = I_0[\exp\left(\frac{qV}{nk_BT}\right) - 1] \tag{1}$$

where I_0, q, n, T, and k_B are the reverse saturation current, the quantity of a positive charge, the ideality factor, the absolute temperature and the Boltzmann constant, respectively. Subsequently, n is determined to be ~2.19 based on equation of $n = \frac{q}{k_BT}\frac{dV}{dlnI}$, which is slightly higher than ideal value (n = 1), but smaller than many reported heterojunction photodetectors based on graphene/GaAs and single-walled carbon nanotube/GaAs heterojunctions [34,35], indicating the high junction quality. In addition, the electrical properties of the junction could be investigated by an equivalent circuit model consisting of a resistor and an ideal diode (the inset of

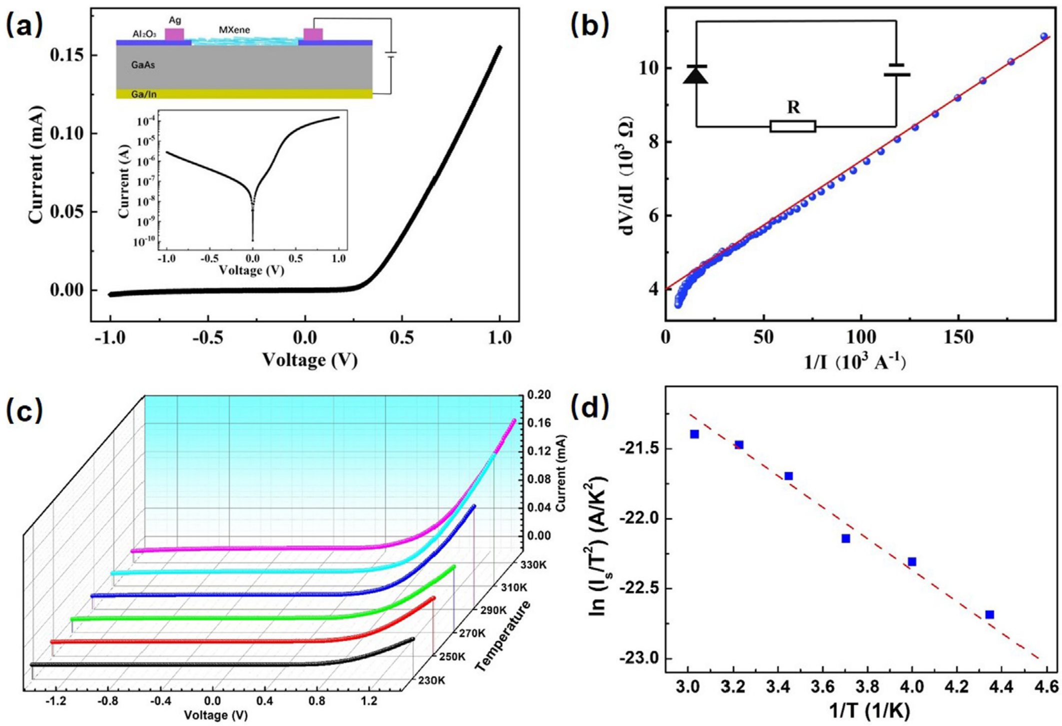

Fig. 3. (a) The *I-V* curve of a typical $Ti_3C_2T_x$/GaAs Schottky junction in the dark at room temperature. The inset depicts the cross-sectional schematic of the device and the semi-logarithmic *I–V* curve. (b) d*V*/d*I* *versus* 1/*I* curve taken from the data in figure (a), the inset shows the equivalent circuit model of the heterojunction consisting of serially connected diode and resistor. (c) The temperature-dependent *I-V* curves in the range of 230–330 K with an interval of 20 K. (d) Richardson plot, $\ln(I_0/T^2)$ *versus* 1000/T for the $Ti_3C_2T_x$/GaAs Schottky junction.

Fig. 3b) [36,37]. The voltage across the resistor and the ideal model could be defined by the following equation:

$$V = IR + \frac{nk_BT}{q}\ln(\frac{I}{I_0}) \quad (2)$$

Moreover, a differential resistance could be obtained by differentiating Eq. (2) with respect to the current.

$$\frac{dV}{dI} = R + \frac{nk_BT}{qI} \quad (3)$$

The d*V*/d*I* *versus* 1/*I* curve is shown in Fig. 3b. Their linear relationship implies that the effectiveness of the equivalent circuit model. Furthermore, the series resistance of the device is deduced to be ~4 KΩ. This value is much lower than that of heterojunction constructed by SnO_2 nanowire/Si and SWCNTs/SnO_2 and confirms the high-quality Schottky junction electrical performance [38,39].

To better understand the carrier transportation mechanism of the $Ti_3C_2T_x$/GaAs Schottky junction, temperature-dependent electrical measurements have been performed. Fig. 3c shows the temperature-dependent *I-V* curves in the range of 230–330 K with an interval of 20 K. The current gradually raises with the increasing temperature, indicating a good dependence of the electrical transport properties on temperature. According to the Eq. (1) combined with thermionic emission (TE) model, the saturation current can be described as [40,41]:

$$I_0 = A^*T^2[exp\frac{-q\varnothing_B}{kT}] \quad (4)$$

where A, A^*, and$\varnothing_B$ are the effective device area (A = 0.25 cm^2), the effective Richardson constant of the GaAs, and the Schottky barrier height (SBH), respectively. Furthermore, Fig. 3d depicts the Richardson plot of $\ln(I_0/T^2)$ as a function of 1000/T for the $Ti_3C_2T_x$/GaAs Schottky junction, from which one can easily see that the good linearity of the $\ln(I_0/T^2)$ *versus* 1000/T plot between 230 K and 330 K, in good agreement with Richardson-Schottky (RS) model [42]. The effective Richardson constant of A^* could be obtained by Eq. (5):

$$\ln\frac{I_0}{T^2} = \ln(AA^*) - \frac{q\varnothing_B}{kT} \quad (5)$$

From the plot shown in Fig. 3d, the SBH value could be deduced to be ~0.15 eV, while A^* was determined as 1.36 × 10^{-4} A/m^2 K^2. The A^* value obtained here is much lower than the previously reported value of n-type GaAs (0.41 × 10^4 A/m^2 K^2) [43,44]. The large deviation indicates a barrier inhomogeneity and potential fluctuations prevailing at the Schottky interface [45,46].

Furthermore, the photodetection performance of the $Ti_3C_2T_x$/GaAs Schottky junction photodetector was systemically evaluated by using a 650 nm laser diode (LD). Panel a and b of Fig. 4 depict the *I-V* curves under the dark condition and 650 nm light illumination with different light intensities from 4.5 μW/cm^2 to 15.2 mW/cm^2. Apparently, the current in reverse bias region is found to increase sharply with the increase of light intensity. Careful examination finds that the device shows an obvious photovoltaic effect with an open-circuit voltage (V_{OC}) of 0.37 V and a short circuit current (I_{SC}) of 7.94 × 10^{-5} A at a light intensity of 15.2 mW/cm^2, rendering the photodetector operate in self-driven mode. On the other hand, The I_{light}/I_{dark} ratio of the $Ti_3C_2T_x$/GaAs Schottky junction as a function of various light intensities is shown in Fig. 4c. Under the same light intensity, the device shows the maximum I_{light}/I_{dark} ratio at zero bias. Specially, the I_{light}/I_{dark} ratio at zero bias increases with the increase of the light intensity, ranging from 5.7 × 10^2 at 4.5 μW/cm^2 to 5.6 × 10^5 at 15.2 mW/cm^2. The corresponding photovoltaic photoresponse of the photodetector under a pulsed 650 nm light irradiation with various power intensities was studied in Fig. 4d. Obviously, the $Ti_3C_2T_x$-based Schottky junction photodetector can be easily and reversibly switched between high and low current states with excellent reproducibility and stability, yielding the highest I_{light}/I_{dark} ratio of 5.6 × 10^5 at light intensity

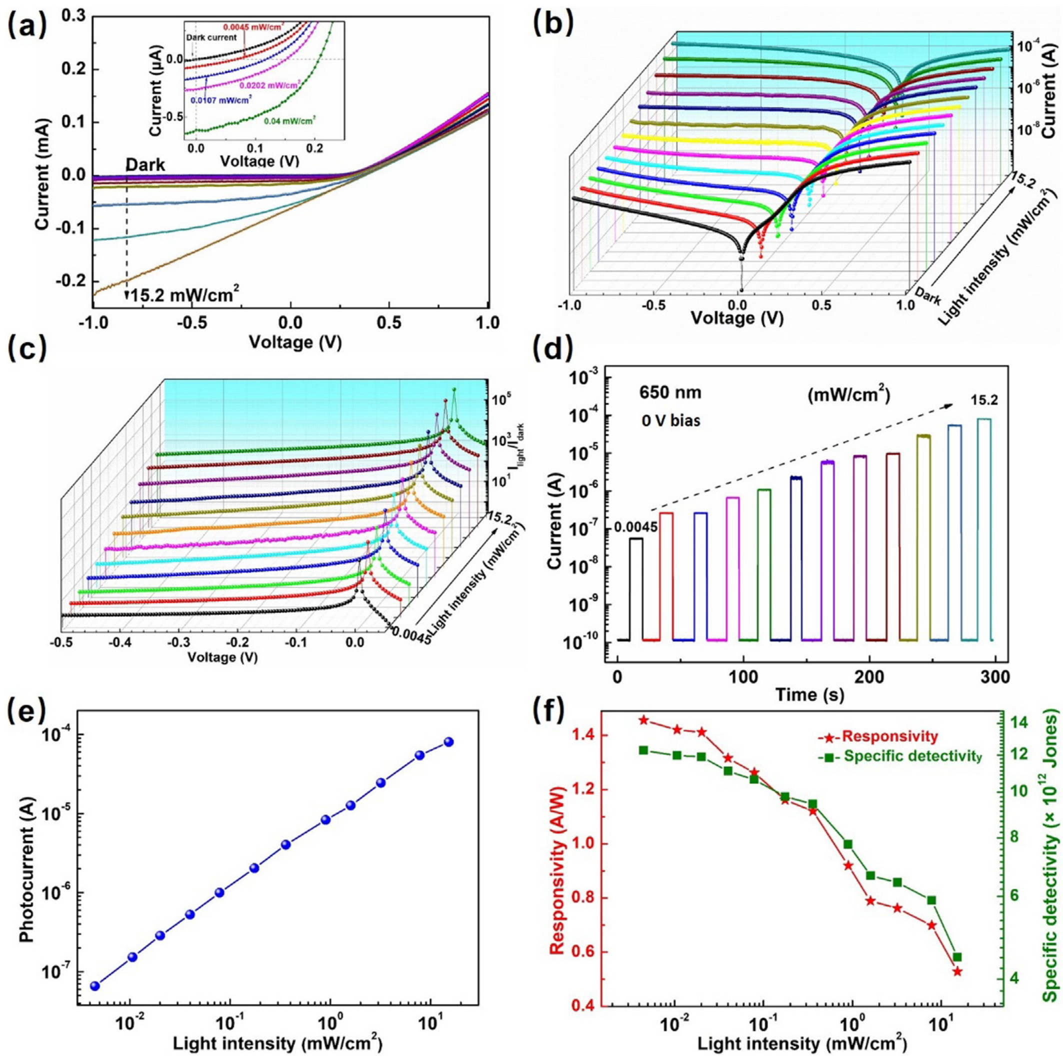

Fig. 4. (a) The *I-V* curves under the dark condition and 650 nm light illumination with various light intensity from 4.5 μW/cm^2 to 15.2 mW/cm^2. The inset of figure (a) shows the *I-V* curves under 650 nm light illumination with some low light intensities. (b) The light intensity dependent *I-V* curves in semi-log coordinates. (c) The I_{light}/I_{dark} ratio of the $Ti_3C_2T_x$/GaAs Schottky junction with various light intensities. (d) Photovoltaic photoresponse of the photodetector under a pulsed 650 nm light irradiation with various power intensities. (e) Plots of the photocurrent as a function of light intensity. (f) Light intensity-dependent responsivity and specific detectivity.

of 15.2 mW/cm^2. Importantly, $I_{\text{light}}/I_{\text{dark}}$ ratio could be as high as 5.7×10^2 at a very low power intensity of 4.5 μW/cm^2, suggesting the perspective of weak light signal detection. Furthermore, the photocurrent defined as difference of current under light illumination and dark condition (I_{ph}, $I_{ph} = I_{light} - I_{dark}$) at zero bias *versus* the incident light intensity (P) is presented in Fig. 4d and e. By analyzing the dependence of photocurrent on light intensity with the use of a power law of $I_{ph} \propto P^{\theta}$ (θ determines the photoresponse to light intensity), a power exponent of θ = 0.95 is obtained [47]. This calculated value is very close to 1, indicating the presence of some trap states between the conduction band edge and the Fermi level [48].

To quantitatively characterize the photodetection performance of the self-driven $Ti_3C_2T_x$/GaAs Schottky junction photodetector, two important figures of merit such as responsivity (R) and specific detectivity (D^*) are calculated according to the following equations [49,50]:

$$R = I_{ph}/PS \tag{6}$$

$$D^* = \sqrt{\frac{A}{2qI_{dark}}}R \tag{7}$$

where S and A are the effective illuminated area (0.01 cm^2) and the effective device area (0.25 cm^2), respectively. Both R and D^* as a function of the incident light intensity (650 nm, zero bias) are plotted in Fig. 4f. It is observed that both values show the decreasing intendency with the increase of light intensity, which could be attributed to the intensified carrier recombination at a higher light intensity [51]. Specifically, the maximum R and D^* of the $Ti_3C_2T_x$-based device are deduced to be 1.46 A/W and 1.23×10^{13} Jones (1 Jones = 1 cm Hz$^{1/2}$ W^{-1}) at a relatively low light intensity of 4.5 μW/cm^2, respectively, which are not only superior to previously reported GaAs-based Schottky junction photodetectors, but also much better than optoelectronic devices based on Mxenes (Table 1) [14,23,24,34,35,52].

The photoresponse properties of the $Ti_3C_2T_x$/GaAs Schottky junction photodetector are found to greatly depend on the incident light. Fig. 5a depicts the time-dependent photovoltaic photoresponse of the device under different wavelength light signals. It is obvious that the device shows the fast response to light signal from 405 nm to 980 nm, suggesting the $Ti_3C_2T_x$/GaAs Schottky junction photodetector is highly sensitive over a multiple spectrum range. As a matter of fact, with the reduction of the light intensities for different wavelengths, the photocurrents also decrease mono-

Table 1
Comparison of the device performance of MXene-based and GaAs-based photodetectors.

Device structre	Response wavelength (nm)	I_{light}/I_{dark} Ratio	Responsivity	Detectivity(Jones)	Self-driven?	Refs
$Ti_3C_2T_x$/GaAs Schottky junction photodetector	405–980	5.6×10^5	1.46 A/W	1.23×10^{13}	Yes	This work
$Ti_3C_2T_x$/n-Si Schottky junction photodetector	405	10^5	26.95 mA/W	–	Yes	[14]
Mxene-GaAs-Mxene Photodetector	532, 780, 830	_–	278 mA/W	11.6×10^{10}	No	[23]
Perovskite/MXene-Based Photodetector	450	2.3×10^3	44.9 mA/W	6.4×10^8	No	[24]
Graphene/AlO_x/GaAs photodetector	850	10^5	5 mA/W	2.98×10^{11}	Yes	[34]
SWCNT/GaAs Heterojunction photodetector	405–1064	–	274 mA/W	7.6×10^{12}	Yes	[35]
AgNPs/graphene/GaAs heterostructure photodetector	325–980	–	210 mA/W	2.98×10^{13}	Yes	[52]

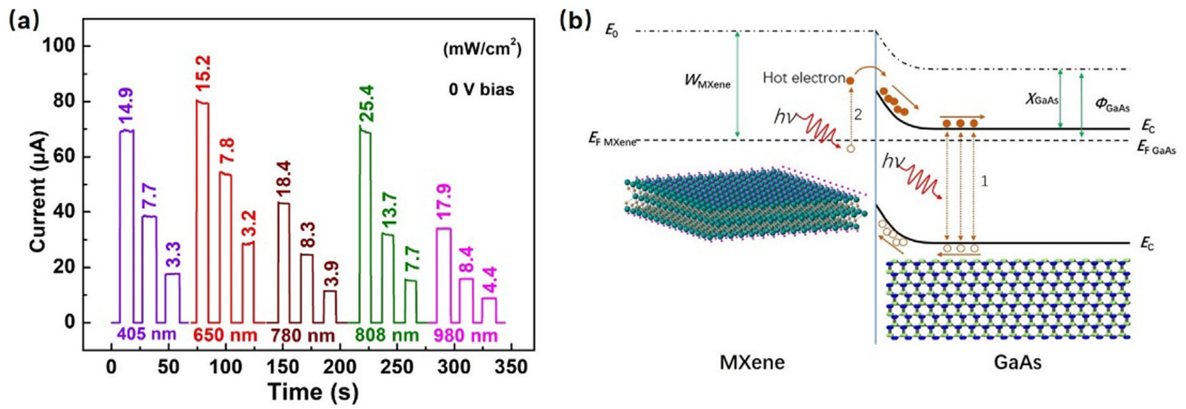

Fig. 5. (a) The time-dependent photovoltaic photoresponse of the device under different wavelength light signals. (b) The energy band diagram of the $Ti_3C_2T_x$/GaAs Schottky junction.

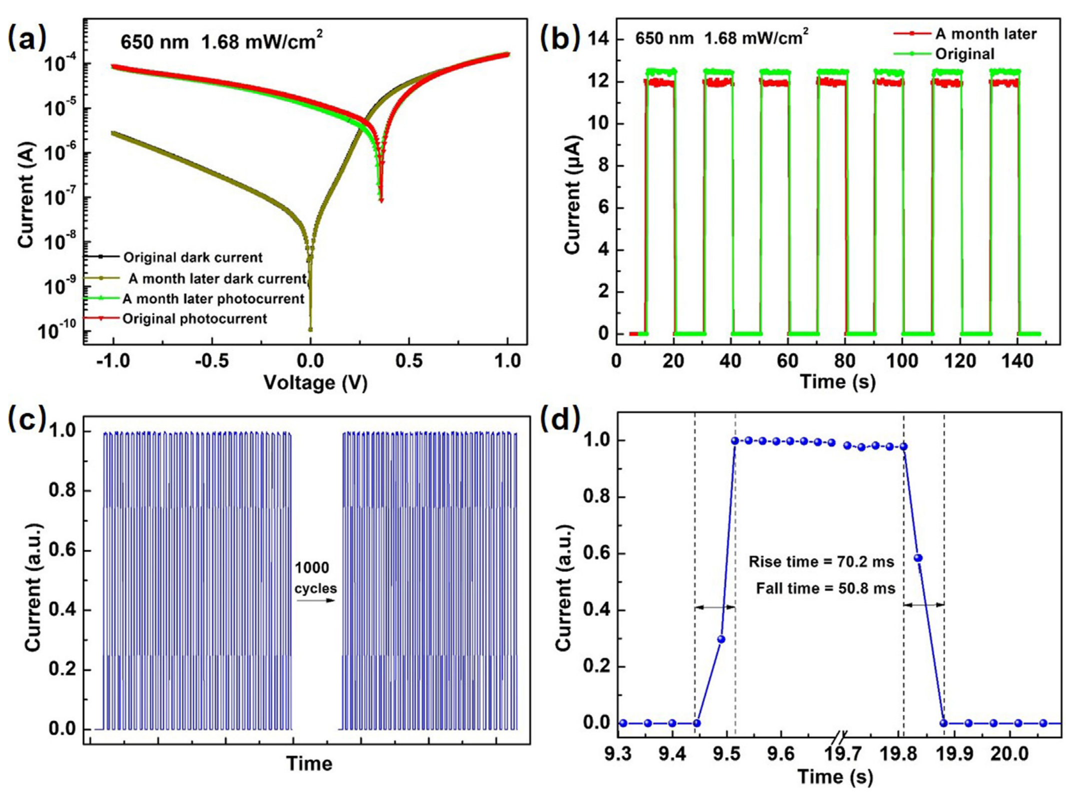

Fig. 6. (a and b) *I-V* characteristics and time-dependent photoresponses of the $Ti_3C_2T_x$/GaAs Schottky junction photodetector after a month storage in air condition. (c) Stability of the $Ti_3C_2T_x$/GaAs Schottky junction photodetector with more than 1000 cycles. (d) One normalized cycle measured to estimate rise/fall time.

tonously. The current is found to raise from 1.43×10^{-10} A to 6.97×10^{-5} A (405 nm, 14.9 mW/cm^2), 7.94×10^{-5} A (650 nm, 15.2 mW/cm^2), 4.32×10^{-5} A (780 nm, 18.4 mW/cm^2), 6.89×10^{-5} A (808 nm, 25.4 mW/cm^2), and 3.40×10^{-5} A (980 nm, 17.9 mW/cm^2), respectively, giving rise to a highest I_{light}/I_{dark} ratio of 5.6×10^5 at 650 nm (15.2 mW/cm^2). It should be noted that the device exhibits a high sensitivity to 980 nm light illumination, which exceeds the absorption edge of GaAs (874 nm), indicating that the photocurrent maybe result from the response of single $Ti_3C_2T_x$ MXene component. The above photoresponse characteristics can be further better understood by the energy band diagram illustrated in Fig. 5b. Because of the work function difference between GaAs and $Ti_3C_2T_x$, the built-in potential across the depletion region would be formed at $Ti_3C_2T_x$/GaAs interface when both materials are contacted. Therefore, upon light illumination in the range of UV-NIR, the light is absorbed by both materials and then photogenerated carriers will be separated and collected by external electrodes, giving rise to the photocurrent in the external circuit. On the other hand, for the light with photon energy smaller than the corresponding bandgap of GaAs, $Ti_3C_2T_x$ would mainly absorb the incident light, hot electrons excited in $Ti_3C_2T_x$ can overcome the Schottky barrier, rendering the device capable of detecting the light with wavelength of up to 980 nm. In addition, plasmon-induced hot electrons in $Ti_3C_2T_x$ MXene film are also responsible for infrared photoresponse. Obviously, the $Ti_3C_2T_x$ MXene film on GaAs is composed of the disordered stacking few layer nanoflakes. The dimensions of these nanoflakes are about several hundreds of nanometers with naturally high density of edges and nanometric gaps, which are considered to efficiently relax plasmonic momentum constraints and promote energized hot electron generation [15]. Consequently, the plasmon-induced hot electrons could be excited and then transit across the Schottky barrier under infrared light and then contribute to the photocurrent.

The long-term stability is also an important factor of photodetector for technological application. Thereby, in order to investigate the ambient stability of our $Ti_3C_2T_x$/GaAs Schottky junction photodetector, the device sample has been stored in the ambient condition without any encapsulation within one month. Intriguingly, the present device exhibits very good stability and only 3.20% decrease in the photocurrent, as shown in Fig. 6a and b. More importantly, even after more than 1000 cycles in a consecutive operation, the device can not only operate very well, but also remain its initial infrared photoresponse properties. Such good device stability could be ascribed to the excellent air stability of $Ti_3C_2T_x$ and high-quality $Ti_3C_2T_x$/GaAs Schottky junction. The rise/fall time is as fast as 70.2/50.8 ms based on the response speed definition. This fast response speed is easily attributed to the strong built-in electric field at the junction interface which is conducive to the quick separation and transport of photo-generated carriers.

4. Conclusion

In summary, we have demonstrated a high-performance broadband and self-driven $Ti_3C_2T_x$/GaAs Schottky junction photodetector by simply dripping $Ti_3C_2T_x$ MXene solution on a pre-defined GaAs substrate. Temperature-dependent electrical measurements were firstly conducted to demonstrate the high-quality Schottky junction electrical performance. The assembled $Ti_3C_2T_x$/GaAs Schottky junction exhibits a pronounced photovoltaic behavior, enabling the device operate in self-driven mode without external energy consumption. What's more, the prominent photodetection properties, including a good responsivity of ~1.46 A/W, an impressive specific detectivity of $\sim 1.23 \times 10^{13}$ Jones, a high I_{light}/I_{dark} ratio of 5.6×10^5 are obtained, which are superior to most of MXene based photodetectors. Significantly, owing to the broad absorption of $Ti_3C_2T_x$ MXene film our photodetector can detect infrared light with wavelength of to 980 nm exceeding the absorption edge of GaAs (874 nm). We believe all these impressive results confirm that the design of novel $Ti_3C_2T_x$/GaAs Schottky junction device show the important application in the field of optoelectronics devices.

CRediT authorship contribution statement

Xiwei Zhang: Methodology, Writing - original draft, Funding acquisition. **Jiahua Shao:** Investigation, Data curation, Writing - review & editing. **Chenxi Yan:** Methodology, Writing - review & editing. **Xinmiao Wang:** Methodology, Writing - review & editing. **Yufei Wang:** Methodology, Writing - review & editing. **Zhihui Lu:** Methodology, Writing - review & editing. **Ruijie Qin:** Methodology, Writing - review & editing. **Xiaowen Huang:** Writing - review & editing. **Junlong Tian:** Funding acquisition, Writing - review & editing. **Longhui Zeng:** Writing - review & editing.

Declaration of Competing Interest

The authors declare that they have no known competing financial interests or personal relationships that could have appeared to influence the work reported in this paper.

Acknowledgements

This work was supported by the key scientific research projects in universities of Henan Province (nos. 20A140001), the Foundation for University Youth Key Teacher by the Henan Province (nos. 2020GGJS186), the Natural Science Foundation of Henan Province (nos. 202300410026), the special Program for Basic Research of the Key Scientific Research Projects in Universities of Henan Province (21zx015), the undergraduate innovation fund of Anyang Normal University (nos. X2020104799098, X2020104790110), the National Natural Science Foundation of China (Grant No. 32001020), Shandong Provincial Natural Science Foundation (ZR2020QB131), Key R&D Program of Shandong Province (2020CXGC011304), and the Qilu University of Technology (Shandong Academy of Sciences) Foundation (202004, 2020KJC-YJ03 and 2020KJC-YJ04).

References:

[1] M. Naguib, M. Kurtoglu, V. Presser, J. Lu, J. Niu, M. Heon, L. Hultman, Y. Gogotsi, M.W. Barsoum, Two-dimensional nanocrystals produced by exfoliation of Ti_3AlC_2, Adv. Mater. 23 (2011) 4278.

[2] M. Naguib, V.N. Mochalin, M.W. Barsoum, Y. Gogotsi, MXenes: a new family of two-dimensional materials, Adv. Mater. 26 (2014) 992.

[3] B. Anasori, M.R. Lukatskaya, Y. Gogotsi, 2D metal carbides and nitrides (MXenes) for energy storage, Nat. Rev. Mater. 2 (2017) 16098.

[4] K. Hantanasirisakul, Y. Gogotsi, Electronic and optical properties of 2D transition metal carbides and nitrides (MXenes), Adv. Mater. 30 (2018) 1804779.

[5] X. Jiang, A.V. Kuklin, A. Baev, Y. Ge, H. Ågren, H. Zhang, P.N. Prasad, Two-dimensional MXenes: from morphological to optical, electric, and magnetic properties and applications, Physics Reports 848 (2020) 1–58.

[6] H. Xu, A. Ren, J. Wu, Z. Wang, Recent advances in 2D MXenes for photodetection, Adv. Funct. Mater. 30 (2020) 2000907.

[7] M. Li, J. Lu, K. Luo, Y. Li, K. Chang, K. Chen, J. Zhou, J. Rosen, L. Hultman, P. Eklund, P.O.Å. Persson, S. Du, Z. Chai, Z. Huang, Q. Huang, Element replacement approach by reaction with Lewis acidic molten salts to synthesize nanolaminated MAX phases and MXenes, J. Am. Chem. Soc. 141 (2019) 4730–4737.

[8] R. Li, L. Zhang, L. Shi, P. Wang, MXene Ti_3C_2: an effective 2D light-to-heat conversion material, ACS Nano 11 (2017) 3752–3759.

[9] H.C. Fu, V. Ramalingam, H. Kim, C.H. Lin, X. Fang, H.N. Alshareef, J.H. He, MXene-contacted silicon solar cells with 11.5% efficiency, Adv. Energy Mater. 9 (2019) 1900180.

[10] Y. Li, H. Shao, Z. Lin, J. Lu, L. Liu, B. Duployer, P.O.Å. Persson, Per Eklund, L. Hultman, M. Li, K. Chen, X.-H. Zha, S. Du, P. Rozier, Z. Chai, E. Raymundo-Piñero, P.-L. Taberna, P. Simon, Q. Huang, A general Lewis acidic etching route for preparing MXenes with enhanced electrochemical performance in non-aqueous electrolyte, Nat. Mater. 19 (2020) 894–899.

[11] C. Xu, L. Wang, Z. Liu, L. Chen, J. Guo, N. Kang, X.L. Ma, H.M. Cheng, W. Ren, Large-area high-quality 2D ultrathin Mo2C superconducting crystals, Nat. Mater. 14 (2015) 1135–1141.

[12] K. Hantanasirisakul, M.Q. Zhao, P. Urbankowski, J. Halim, B. Anasori, S. Kota, C. E. Ren, M.W. Barsoum, Y. Gogotsi, Fabrication of $Ti_3C_2T_x$ MXene transparent thin films with tunable optoelectronic properties, Adv. Electron. Mater. 2 (2016) 1600050.

[13] C.F. Zhang, B. Anasori, A. Seral-Ascaso, S.H. Park, N. McEvoy, A. Shmeliov, G.S. Duesberg, J.N. Coleman, Y. Gogotsi, V. Nicolosi, Transparent, flexible, and conductive 2D titanium carbide (MXene) films with high volumetric capacitance, Adv. Mater. 29 (2017) 1702678.
[14] Z. Kang, Y. Ma, X. Tan, M. Zhu, Z. Zheng, N. Liu, L. Li, Z. Zou, X. Jiang, T. Zhai, Y. Gao, MXene–silicon Van Der Waals heterostructures for high-speed self-driven photodetectors, Adv. Electron. Mater. 3 (2017) 1700165.
[15] D.B. Velusamy, J.K. El-Demellawi, A.M. El-Zohry, A. Giugni, S. Lopatin, M.N. Hedhili, A.E. Mansour, E.D. Fabrizio, O.F. Mohammed, H.N. Alshareef, MXenes for plasmonic photodetection, Adv. Mater. 31 (2019) 1807658.
[16] X. Zhang, J. Shao, C. Yan, R. Qin, Z. Lu, H. Geng, T. Xu, L. Ju, A review on optoelectronic device applications of 2D transition metal carbides and nitrides, Mater. Des. 200 (2021) 109452.
[17] N.K. Chaudhari, H. Jin, B. Kim, D.S. Baek, S.H. Joo, K. Lee, MXene: an emerging two-dimensional material for future energy conversion and storage applications, J. Mater. Chem. A 5 (2017) 24564–24579.
[18] F. Shahzad, M. Alhabeb, C.B. Hatter, B. Anasori, S. Man Hong, C.M. Koo, Y. Gogotsi, Electromagnetic interference shielding with 2D transition metal carbides (MXenes), Science 353 (2016) 1137–1140.
[19] A.D. Dillon, M.J. Ghidiu, A.L. Krick, J. Griggs, S.J. May, Y. Gogotsi, M.W. Barsoum, A.T. Fafarman, Highly conductive optical quality solution-processed films of 2D titanium carbide, Adv. Funct. Mater. 26 (2016) 4162–4168.
[20] S. Ahn, T.-H. Han, K. Maleski, J. Song, Y.-H. Kim, M.-H. Park, H. Zhou, S. Yoo, Y. Gogotsi, T.-W. Lee, A 2D titanium carbide MXene flexible electrode for high-efficiency light-emitting diodes, Adv. Mater. 32 (2020) 2000919.
[21] L.-H. Zeng, S.-H. Lin, Z.-J. Li, Z.-X. Zhang, T.-F. Zhang, C. Xie, C. Hi Mak, Y. Chai, S. P. Lau, L.-B. Luo, Y.H. Tsang, Fast, self-driven, air-stable, and broadband photodetector based on vertically aligned $PtSe_2$/GaAs heterojunction, Adv. Funct. Mater. 28 (2018) 1705970.
[22] R. Zhuo, L. Zeng, H. Yuan, D. Wu, Y. Wang, Z. Shi, T. Xu, Y. Tian, X. Li, Y.H. Tsang, In-situ fabrication of $PtSe_2$/GaN heterojunction for self-powered deepultraviolet photodetector with ultrahigh current on/off ratio and detectivity, Nano Res. 12 (2019) 183–189.
[23] K. Montazeri, M. Currie, L. Verger, P. Dianat, M.W. Barsoum, B. Nabet, Beyond gold: spin-coated Ti3C2-based MXene photodetectors, Adv. Mater. 31 (2019) 1903271.
[24] W. Deng, H. Huang, H. Jin, W. Li, X. Chu, D. Xiong, W. Yan, F. Chun, M. Xie, C. Luo, L. Jin, C. Liu, H. Zhang, W. Deng, W. Yang, All-sprayed-processable, large-area, and flexible perovskite/MXene-based photodetector arrays for photocommunication, Adv. Optic. Mater. 7 (2019) 1801521.
[25] Z. Kang, Y. Cheng, Z. Zheng, F. Cheng, Z. Chen, L. Li, X. Tan, L. Xiong, T. Zhai, Y. Gao, MoS_2-based photodetectors powered by asymmetric contact structure with large work function difference, Nano-Micro Lett. 11 (2019) 34.
[26] J. Chen, Z. Li, F. Ni, W. Ouyanga, X. Fang, Bio-inspired transparent MXene electrodes for flexible UV photodetectors, Mater. Horiz. 7 (2020) 1828–1833.
[27] T. Jiang, Y. Huang, X. Meng, CdS core-Au/MXene-based photodetectors: positive deep-UV photoresponse and negative UV–Vis-NIR photoresponse, Appl. Surf. Sci. 513 (2020) 145813.
[28] S. Guo, S. Kang, S. Feng, W. Lu, MXene-enhanced deep ultraviolet photovoltaic performances of crossed Zn_2GeO_4 nanowires, J. Phys. Chem. C 124 (2020) 4764–4771.
[29] W. Ouyang, J. Chen, J.H. He, X. Fang, Improved photoelectric performance of UV photodetector based on ZnO nanoparticle-decorated BiOCl nanosheet arrays onto PDMS substrate: the heterojunction and $Ti_3C_2T_x$ MXene conduction layer, Adv. Electron. Mater. 6 (2020) 2000168.
[30] Y. Yang, J. Jeon, J.-H. Park, M.S. Jeong, B.H. Lee, E. Hwang, S. Lee, Plasmonic transition metal carbide electrodes for high-performance InSe photodetectors, ACS Nano 13 (2019) 8804–8810.
[31] J. Luo, W. Zhang, H. Yuan, C. Jin, L. Zhang, H. Huang, C. Liang, Y. Xia, J. Zhang, Y. Gan, X. Tao, Pillared structure design of MXene with ultralarge interlayer spacing for high-performance lithium-ion capacitors, ACS Nano 11 (2017) 2459–2469.
[32] J. Halim, M.R. Lukatskaya, K.M. Cook, J. Lu, C.R. Smith, L.-Å. Näslund, S.J. May, L. Hultman, Y. Gogotsi, P. Eklund, M.W. Barsoum, Transparent conductive two-dimensional titanium carbide epitaxial thin films, Chem. Mater. 26 (2014) 2374–2381.
[33] S.A. Shah, T. Habib, H. Gao, P. Gao, W. Sun, M.J. Green, M. Radovic, Template-free 3D titanium carbide ($Ti_3C_2T_x$) MXene particles crumpled by capillary forces, Chem. Commun. 53 (2017) 400–403.
[34] L.-B. Luo, H. Hu, X.-H. Wang, R. Lu, Y.-F. Zou, Y.-Q. Yu, F.-X. Liang, A graphene/GaAs near-infrared photodetector enabled by interfacial passivation with fast response and high sensitivity, J. Mater. Chem. C 3 (2015) 4723–4728.
[35] T. Huo, H. Yin, D. Zhou, L. Sun, T. Tian, H. Wei, N. Hu, Z. Yang, Y. Zhang, Y. Su, Self-powered broadband photodetector based on single-walled carbon nanotube/GaAs heterojunctions, ACS Sustainable Chem. Eng. 8 (2020) 15532–15539.
[36] K.W. Min, Y.K. Kim, G. Shin, S. Jang, M. Han, J. Huh, G.T. Kim, J.S. Ha, White-light emitting diode array of p^+-Si/aligned n-SnO_2 nanowires heterojunctions, Adv. Funct. Mater. 21 (2011) 119–124.
[37] X.W. Zhang, X.J. Zhang, L. Wang, Y.M. Wu, Y. Wang, P. Gao, Y.Y. Han, J.S. Jie, ZnSe nanowire/Si p–n heterojunctions: device construction and optoelectronic applications, Nanotechnology 24 (2013) 395201.
[38] M.Y. Bae, K.W. Min, J. Yoon, G.T. Kim, J.S. Ha, Electronic properties of light-emitting p-n hetero-junction array consisting of p^+-Si and aligned n-ZnO nanowires, J. Appl. Phys. 113 (2013) 084310.
[39] J. Yoon, K.W. Min, J. Kim, G.T. Kim, J.S. Ha, p–n hetero-junction diode arrays of p-type single walled carbon nanotubes and aligned n-type SnO_2 nanowires, Nanotechnology. 23 (2012) 265301.
[40] S. Neetika, A. Kumar, H.K. Sanger, A. Chourasiya, K. Kumar, R. Asokan, V.K. Chandra, Malik, Influence of barrier inhomogeneities on transport properties of Pt/MoS2 Schottky barrier junction, J. Alloys Comp. 797 (2019) 582–588.
[41] S.M. Sze, Physics of Semiconductor Devices, second ed., Wiley, New York, 1981.
[42] S.B. Son, Y. Kim, B. Cho, C.-J. Choi, W.-K. Hong, Temperature-dependent electronic charge transport characteristics at MoS_2/p-type Ge heterojunctions, J. Alloys Comp. 757 (2018) 221–227.
[43] D. Tomer, S. Rajput, L.J. Hudy, C.H. Li, L. Li, Inhomogeneity in barrier height at graphene/Si (GaAs) Schottky junctions, Nanotechnology 26 (2015) 215702.
[44] M. Missous, E.H. Rhoderick, On the Richardson constant for aluminum/gallium arsenide Schottky diodes, J. Appl. Phys. 69 (1991) 7142.
[45] Z.J. Horvath, Analysis of I-V measurements on $CrSi_2$-Si Schottky structures in a wide temperature range, Solid-State Electron. 39 (1996) 176–178.
[46] A. Gümüs, A. Türüt, N. Yalçin, Temperature dependent barrier characteristics of CrNiCo alloy Schottky contacts on n-type molecular-beam epitaxy GaAs, J. Appl. Phys. 91 (2002) 245–250.
[47] X. Yu, P. Yu, D. Wu, B. Singh, Q. Zeng, H. Lin, W. Zhou, J. Lin, K. Suenaga, Z. Liu, Q.J. Wang, Atomically thin noble metal dichalcogenide: a broadband mid-infrared semiconductor, Nat. Commun. 9 (2018) 1545.
[48] L.H. Zeng, M.Z. Wang, H. Hu, B. Nie, Y.Q. Yu, C.Y. Wu, L. Wang, J.G. Hu, C. Xie, F. X. Liang, L.B. Luo, Monolayer Graphene/Germanium Schottky junction as high-performance self-driven infrared light photodetector, ACS Appl. Mater. Interfaces 5 (2013) 9362–9366.
[49] C. Ling, T. Guo, W. Lu, Y. Xiong, L. Zhu, Q. Xue, Ultrahigh broadband photoresponse of SnO_2 nanoparticle thin film/SiO_2/p-Si heterojunction, Nanoscale 9 (2017) 8848–8857.
[50] J. Yao, Z. Deng, Z. Zheng, G. Yang, Stable, fast UV–Vis–NIR photodetector with excellent responsivity, detectivity, and sensitivity based on α-In_2Te_3 films with a direct bandgap, ACS Appl. Mater. Inter. 8 (2016) 20872–20879.
[51] L. Zeng, S. Lin, Z. Li, Z. Zhang, T. Zhang, C. Xie, C. Mak, Y. Chai, S.P. Lau, L. Luo, Y. H. Tsang, Fast, self-driven, air-stable, and broadband photodetector based on vertically aligned $PtSe_2$/GaAs heterojunction, Adv. Funct. Mater. 28 (2018) 1705970.
[52] Y. Lu, S. Feng, Z. Wu, Y. Gao, J. Yang, Y. Zhang, Z. Hao, J. Li, E. Li, H. Chen, S. Lin, Broadband surface plasmon resonance enhanced self-powered graphene/GaAs photodetector with ultrahigh detectivity, Nano Energy 47 (2018) 140–149.